Journal of Fluids and Structures 60 (2016) 114–129

Contents lists available at ScienceDirect

Journal of Fluids and Structures

journal homepage: www.elsevier.com/locate/jfs

Drag reduction by elastic reconfiguration of non-uniform beams in non-uniform flows

Tristan Leclercq *, Emmanuel de Langre

Department of Mechanics, LadHyX, CNRS, École Polytechnique, 91128 Palaiseau, France

ARTICLE INFO

Article history:
Received 11 June 2015
Accepted 18 October 2015

Keywords:
Drag reduction
Elastic reconfiguration
Vogel exponent
Non-uniform flow
Self-similarity

ABSTRACT

Flexible systems bending in steady flows are known to experience a lesser drag compared to their rigid counterpart. Through a careful dimensional analysis, an analytical expression of the Vogel exponent quantifying this reduction of drag is derived for cantilever beams, within a framework based on spatial self-similar modelling of the flow and structural properties at the clamped edge of the structure. Numerical computations are performed on various situations, including systems involving more complex distributions of the flow or structural parameters. The scaling of drag versus flow velocity for large loadings is shown to be well predicted by fitting the system properties by simple power laws at the scale of the length on which significant bending occurs. Ultimately, the weak sensitivity of the Vogel exponent to the parameters of the system provides an explanation to the rather reduced scattering of the Vogel exponents around -1 observed on most natural systems in aquatic or aerial vegetation.

1. Introduction

It has been well known, since the seminal work of Vogel (1984), that flexible structures subjected to fast flows experience a drag F that grows slower with the velocity than if they were rigid. When the velocity U of the flow exceeds a given threshold, the classical quadratic velocity–drag law that holds for rigid bodies at large Reynolds number changes to a smaller power law $F \propto U^{2+\nu}$ characterized by the so-called Vogel exponent ν, which is negative. This phenomenon is for instance broadly observed in nature. Indeed, plants growing in fast flow environments are very often made of flexible tissues that bend to comply with the flow, hence lowering the risk of failure by fracture or uprooting.

To get a better understanding of the underlying mechanisms, Alben et al. (2002, 2004) first studied the model problem of an elastic one dimensional fibre in an inviscid two dimensional flow, both experimentally and numerically. Their study revealed the importance of a single control parameter, which they call the elastohydrodynamical number, related to the more commonly used Cauchy number C_Y (Tickner and Sacks, 1969; Chakrabarti, 2002; de Langre, 2008), that scales the competing effects of fluid loading to the elastic restoring force. The model of Alben et al. (2002, 2004) exhibits the expected transition from the classical rigid-body U^2 drag scaling law to a new $U^{4/3}$ drag law concomitant with the convergence towards a self-similar shape at large Cauchy numbers. Gosselin et al. (2010) obtained similar results for a finite width plate with a simplified model of fluid loading. They also managed to predict the same asymptotic drag scaling law from a very simple dimensional analysis. In order to explain the drag reduction due to the rolling up of daffodil leaves originally

* Corresponding author.
E-mail addresses: leclercq@ladhyx.polytechnique.fr (T. Leclercq), delangre@ladhyx.polytechnique.fr (E. de Langre).

http://dx.doi.org/10.1016/j.jfluidstructs.2015.10.007
0889-9746/

observed by Vogel (1984), Schouveiler and Boudaoud (2006) obtained theoretical and experimental estimates of the Vogel exponent for circular plastic sheets cut along a radius. They found a drag scaling as $U^{2/3}$, while a theoretical and numerical study by Alben (2010) on the same system concludes that the drag increases as U^1. Recent studies have proposed models that account for additional effects such as gravity (Luhar and Nepf, 2011), viscosity (Zhu and Peskin, 2007; Zhu, 2008), shear background flow (Henriquez and Barrero-Gil, 2014) or unsteady wake effects due to vortex shedding at the edges (Yang et al., 2014).

Many experimental measurements made either in the field or in the laboratory have also been able to provide estimates of the Vogel exponents for systems as diverse as full trees, grasses, flowers, leaves, near-shore marine macrophytes or freshwater algae. Some quite comprehensive reviews such as Harder et al. (2004) or de Langre et al. (2012) list Vogel exponents varying in a range around -0.7, between 0 and -1.3 at most for such systems. What is especially striking is not the scattering of Vogel exponents found for different systems, but much more the robustness of the drag reduction phenomenon with respect to the great variability of structural and flow configurations, and the rather narrow range in which the Vogel exponents usually lie. From the assumption that the scaling of drag reduction results from the loss of one typical length scale, de Langre et al. (2012) showed that the Vogel exponent of any structure made of beams and plates (such as most plants) should exhibit approximately the same behaviour. By a simple dimensional analysis, they recovered the classical $-2/3$ Vogel exponent found by Alben et al. (2002, 2004) and Gosselin et al. (2010). They further claimed that non-linearity in the material constitutive law should have little impact on the scaling of drag. Any possible effect of flow or structural non-uniformities was however not addressed in this study, and nor was it, to the authors' knowledge, in any other one, with the only exception of Henriquez and Barrero-Gil (2014) in the specific case of shear flow. A range of models is clearly missing to fill the gap between the idealized cases above and the more complex natural configurations.

The goal of the present work is to provide a general framework for the derivation of the Vogel exponent of a flexible beam in the limit of large velocity flows. It includes most possible non-uniformities in the flow or structural parameters, but it excludes the additional effects of viscosity, unsteadiness in the wake or in the background flow, or other external forces such as gravity. In some aspects, it is a generalization of the works of Gosselin et al. (2010), de Langre et al. (2012) and Luhar and Nepf (2011).

In Section 2, the general framework of this study is described. In Section 3, a theoretical analysis of drag reduction of a system described by self-similar fluid and structural parameters is presented. In Section 4, the results of numerical simulations performed on several practical cases are given. Finally, Section 5 discusses the implications of the present results regarding the understanding and the predictability of the typical values of the Vogel exponents of actual systems. A nomenclature of the main variables used throughout this paper is given in Table 1.

2. Model

The model used in this paper is represented in Fig. 1. The elastic body is a cantilever beam of length L bending in the xz-plane. The width W, thickness D and material stiffness may all vary with the curvilinear coordinate s. The height $z(s)$ and

Table 1
Nomenclature.

L, $W(s)$, $D(s)$	Length, width and thickness of the beam
$EI(s)$	Bending stiffness in the case of linear elasticity
$C_D(s)$	Cross-section drag coefficient
$\rho(z)$	Fluid density distribution
$U(z)$, U_0	Flow profile and reference velocity
$\theta(s)$, $\kappa(s)$	Inclination angle of the beam from the vertical axis and curvature
$m(s)$, m_0	Internal bending moment and reference value
$f_n(s)$	Internal shear force
$q(s)$, q_0	Local normal fluid load and reference value
$c(\theta)$	Angular dependence of the normal fluid load
$g(\kappa)$, α	Function and exponent associated with the material constitutive law
$b(s)$, b_0, β	Distribution, reference and exponent associated with the stiffness factor
$w(s)$, w_0, γ	Distribution, reference and exponent associated with the cross-section shape factor
$p(z)$, p_0, μ	Distribution, reference and exponent associated with the pressure
ϕ, ψ	Geometrical and material parameter
F, F_{rigid}	Drag force on the flexible/rigid beam
$\mathcal{R}$	Reconfiguration number
C_Y	Cauchy number
ν, ν_∞	Local and asymptotic Vogel exponents
ℓ	Characteristic non-dimensional bending length
L_B	Characteristic non-dimensional boundary layer thickness
δ	Characteristic non-dimensional tapering length

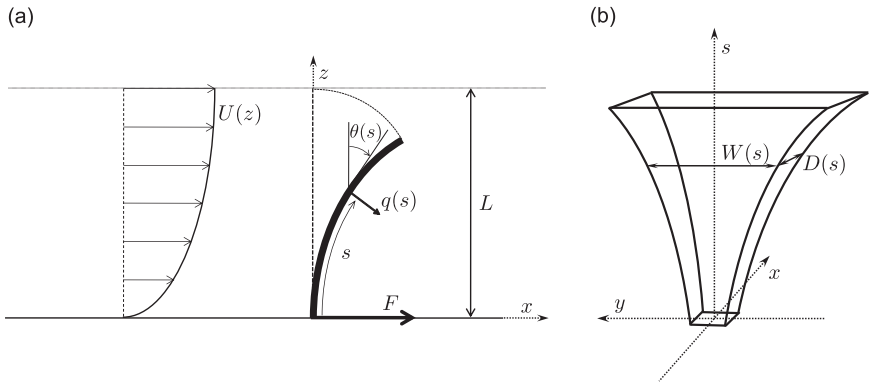

Fig. 1. Description of the system. (a) Side view of the beam bending in the flow. (b) Front view of the unbent structure.

curvature $\kappa(s)$ are related to the local angle of the beam with the vertical axis $\theta(s)$ by the kinematic relationships:

$$z = \int_0^s \cos\ \theta(s')\, ds', \quad \kappa = \frac{\partial \theta}{\partial s}. \tag{1}$$

We assume a rather general form of the constitutive law relating the internal bending moment m to the curvature κ:

$$m(s,\kappa) = b(s)g(\kappa), \tag{2}$$

where $b(s)$ is a local coefficient that accounts for the local stiffness and geometry, while $g(\kappa)$ is characteristic of the material constitutive law, which we take to be uniform on the beam. For instance, in the case of linear elasticity, $g(\kappa)=\kappa$ and $b(s)=EI(s)$ is the local bending stiffness of the beam. Under the assumption that the local radius of curvature $1/\kappa$ remains large compared to the thickness D ($\kappa D \ll 1$), Kirchoff's equations for rods (see for instance Audoly and Pomeau, 2010) relates the internal shear force f_n to the internal bending moment m by

$$f_n = -\frac{\partial m}{\partial s}. \tag{3}$$

We further assume that the structure is placed in a horizontal flow $U(z)$ of a fluid of density $\rho(z)$. Both U and ρ may vary with the vertical coordinate z, Fig. 1a only displaying a velocity profile $U(z)$ for clarity. We restrict our study to large Reynolds numbers, so that viscosity effects are neglected. The local fluid load q is then purely normal. In the case of uniform flow, it is usually considered that the normal fluid load includes one term due to the so-called "reactive force" ($\sim \rho U^2 W D\kappa$ in the steady limit of the model of Lighthill, 1971, see also Candelier et al., 2011) and one other term due to flow separation ("resistive force" $\sim \rho U^2 W$ in the model of Taylor, 1952). Thus, in the slender body assumption $\kappa D \ll 1$, the resistive force is dominant. We assume that this is still the case for our vertically varying flow, and so we take q as purely resistive and independent of the body curvature. We assume a somewhat general form

$$q(s,z,\theta) = p(z)w(s)c(\theta), \tag{4}$$

where $p(z)$ accounts for the local dynamic pressure due to the undisturbed background flow at height z on the beam, $w(s)$ is a shape coefficient that accounts for the interactions of the normal flow with the local cross-section, and $c(\theta)$ is a projection term due to the local angle of the cross-section with respect to the background flow. It is not always obvious that the s- and θ-dependency can be decoupled, as the structure of the boundary layer and of the recirculating flow downstream will be modified by the angle of incidence. However, it is usually considered that to the first order, the resistive normal force only depends on the interaction between the cross-section and the flow in a plane normal to it, hence the expression chosen. The most classical example of such model is the resistive pressure drag derived by Taylor (1952): $q = 1/2\rho C_D W U_n^2$ where ρ is the fluid density, W the local width of the structure, $U_n = U\ \cos\ \theta$ the normal projection of the local flow velocity, and C_D a drag coefficient that accounts for the shape of the local cross-section. Specifically, Taylor's model is equivalent to considering

$$p(z) = \tfrac{1}{2}\rho(z)U^2(z), \quad w(s) = C_D(s)W(s), \quad c(\theta) = \cos^2\theta. \tag{5}$$

Note that the model chosen here only gives an approximation of the exact loading. In particular, the modifications of the flow caused by the structure itself are neglected. However, the close similarity of the results obtained, on the one hand by Gosselin et al. (2010) with the present model, and on the other hand by Alben et al. (2002, 2004) who computed the pressure force distribution on the actual structure using a much more complex algorithm, indicates that the exact form of the force has little impact on the asymptotic scaling of the drag. Unless otherwise stated, $c(\theta) = \cos^2\theta$ is used everywhere in the rest of this paper. The framework of the present paper includes the study of the influence of the still unspecified form of $g(\kappa)$, $b(s)$, $w(s)$, and $p(z) \propto U^2(z)$. Note that the dynamic pressure due to the background flow at a given point in space does not depend on the position of the structure, so $p(z)$ only depends on the Cartesian coordinate z (assuming the flow is invariant in the x-direction). On the other hand, the elasticity factor $b(s)$ and the cross-section shape coefficient $w(s)$ are structural properties that are specific to a given location along the beam span s, even though the Cartesian coordinates (x,z)

of that physical point change as the beam bends. The internal bending moment $m(s)$ depends on the curvilinear coordinate s explicitly via the local stiffness factor $b(s)$, but also implicitly via the local value of the curvature $\kappa(s)$ in the material constitutive law $g(\kappa)$.

Following Luhar and Nepf (2011), the local equilibrium at a given point s^* between the local internal shear force and the normal fluid load yields the governing equation

$$\left.\frac{\partial m}{\partial s}\right|_{s^*} = -\int_{s^*}^{L} q(s)\ \cos\left(\theta(s)-\theta(s^*)\right) ds, \tag{6}$$

where the force-free boundary condition $f_n=0$ at the free end $s=L$ has been used. Non-dimensionalizing this equation yields one governing parameter called the Cauchy number

$$C_Y = \frac{q_0 L}{m_0/L} \sim \frac{\text{typical external fluid load}}{\text{typical elastic restoring force}}, \tag{7}$$

considering that q_0 and m_0 are the orders of magnitude of the fluid load q and internal moment m in Eq. (6). Besides, the total drag of the beam reads

$$F = \int_0^L q(s)\ \cos\left(\theta(s)\right) ds. \tag{8}$$

The focus of this paper is the scaling of the drag force, F, with the velocity of the flow. In the case of a flow that may not be uniform, we have to choose a reference velocity U_0 that scales the velocity at any point in the flow field. We are then interested in the variations of the Vogel exponent ν such that F scales as $U_0^{2+\nu}$, noted $F \propto U_0^{2+\nu}$. At large Reynolds number and in the limit of a rigid structure, the drag force is expected to grow as U_0^2. Following Gosselin et al. (2010), to isolate the contribution of flexibility to the velocity–drag law, we define the reconfiguration number

$$\mathcal{R} = \frac{F}{F_{rigid}}, \tag{9}$$

so that $\mathcal{R} \propto U_0^{\nu}$. The actual governing parameter being the Cauchy number, we will prefer to work in the C_Y–$\mathcal{R}$ space rather than the U_0–F space. The Cauchy number being proportional to the typical fluid load $q_0 \propto U_0^2$, the local Vogel exponent can be computed directly in the C_Y–$\mathcal{R}$ space as

$$\nu = 2\frac{\partial \log \mathcal{R}}{\partial \log C_Y}. \tag{10}$$

A schematic view of the correspondence between the three different representations of a velocity–drag relationship is displayed in Fig. 2 in arbitrary units. The Vogel exponent displayed in Fig. 2c corresponds to twice the slope of the loglog plot $\mathcal{R}(C_Y)$ shown in Fig. 2b. In this particular case, the Vogel exponent asymptotically goes to -1 for large Cauchy numbers, so that the velocity–drag law goes from quadratic to linear.

In the remaining of this paper, unless otherwise stated, the Cauchy number is always defined based on the flow and structural properties at the tip of the upright beam.

3. Drag reduction in a self-similar framework

First, we further assume that the pressure, cross-section shape and stiffness parameters $p(z)$, $w(s)$ and $b(s)$ can be expressed as power functions of their respective arguments, namely

$$p(z) = p_0\left(\frac{z}{L}\right)^{\mu}, \quad w(s) = w_0\left(\frac{s}{L}\right)^{\gamma}, \quad b(s) = b_0\left(\frac{s}{L}\right)^{\beta}. \tag{11}$$

Note that, although these power-law formulations of the structural parameters w and b may recall those of Lopez et al.

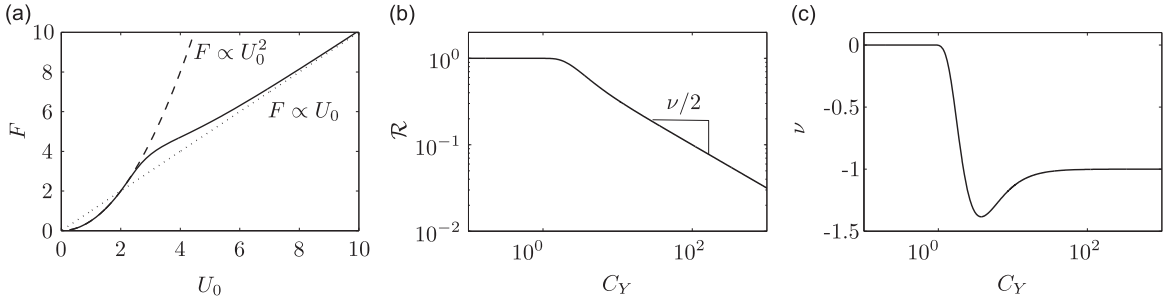

Fig. 2. Schematic view of the loading–drag relationship in the different parameter spaces (arbitrary units). U_0: reference flow velocity, F: drag force, C_Y: Cauchy number, $\mathcal{R}$: Reconfiguration number, and ν: Vogel exponent.

(2011) for a slender cone, or those of Lopez et al. (2014) for a tree-like structure, they actually describe quite different distributions because the curvilinear coordinate s used in these papers was defined from the free tip towards the floor instead of the other way around here. We also assume that the material constitutive law may differ from linear elasticity by considering a more general dependency on curvature, still in the form of a power law

$$g(\kappa) = \kappa^{\alpha}. \tag{12}$$

Substituting (11) and (12) and the particular form $c(\theta) = \cos^2\theta$ into (6), the equilibrium equation reads

$$\frac{\partial}{\partial s}(s^{\beta}\kappa^{\alpha})\bigg|_{s^*} = -C_Y \int_{s^*}^{1} \left(\int_0^s \cos\ \theta(s')\, ds'\right)^{\mu} s^{\gamma}\ \cos^2(\theta)\cos(\theta-\theta^*)\, ds, \tag{13}$$

where all the space variables have been made non-dimensional using the beam length L, and the Cauchy number C_Y has been defined as

$$C_Y = \frac{p_0 w_0 L}{b_0 L^{-1-\alpha}}. \tag{14}$$

From (8), the total drag force on the beam in this framework reads

$$F = p_0 w_0 L \int_0^1 \left(\int_0^s \cos\ \theta(s')\, ds'\right)^{\mu} s^{\gamma} \cos^3(\theta)\, ds. \tag{15}$$

We further assume that the drag is bounded by that on a rigid structure, namely

$$F_{rigid} = p_0 w_0 L \int_0^1 s^{\mu+\gamma}\, ds = \frac{p_0 w_0 L}{1+\mu+\gamma}. \tag{16}$$

For this quantity to be finite, it is required that $\mu+\gamma > -1$. Using (9), (15) and (16), the reconfiguration number now reads

$$\mathcal{R} = (1+\mu+\gamma) \int_0^1 \left(\int_0^s \cos\ \theta(s')\, ds'\right)^{\mu} s^{\gamma}\ \cos^3(\theta)\, ds. \tag{17}$$

Within this framework, the asymptotic Vogel exponent for large Cauchy numbers, noted ν_∞, can now be inferred from a dimensional analysis that accounts for the particular power-like form of the flow and structural parameters. The flow pressure p, the cross-section shape coefficient w and the bending stiffness b are characterized by their respective invariants:

$$\begin{aligned} I_p &= \frac{p(z)}{z^{\mu}} = \frac{p_0}{L^{\mu}}\ [\mathrm{kg\ m^{-1-\mu}\ s^{-2}}], \\ I_w &= \frac{w(s)}{s^{\gamma}} = \frac{w_0}{L^{\gamma}}\ [\mathrm{m^{1-\gamma}}], \\ I_b &= \frac{b(s)}{s^{\beta}} = \frac{b_0}{L^{\beta}}\ [\mathrm{kg\ m^{2+\alpha-\beta}\ s^{-2}}]. \end{aligned} \tag{18}$$

The Vaschy–Buckingham theorem predicts three non-dimensional figures which we choose to be the non-dimensional drag force, the Cauchy number and the aspect ratio:

$$\tilde{F} = \frac{F}{I_p I_w L^{1+\mu+\gamma}}, \quad C_Y = \frac{I_p I_w L^{1+\mu+\gamma}}{I_b L^{-1-\alpha+\beta}}, \quad \Lambda = \frac{w_0}{L}. \tag{19}$$

Following Gosselin et al. (2010), we disregard the effect of the aspect ratio Λ so that the problem reduces to finding the relationship between $\tilde{F}$ and C_Y, or equivalently to determining the function $\mathcal{G}$ such that

$$F = I_p I_w L^{1+\mu+\gamma} \mathcal{G}\left(\frac{I_p I_w}{I_b} L^{2+\mu+\gamma+\alpha-\beta}\right). \tag{20}$$

For highly bent structures, Gosselin et al. (2010) demonstrated that the drag no longer depends on the beam length L. Hence, function $\mathcal{G}$ must be taken as a power function $\mathcal{G}(C_Y) \propto C_Y^{\varphi}$ that cancels the overall exponent of L in (20), meaning

$$(1+\mu+\gamma) + \varphi(2+\mu+\gamma+\alpha-\beta) = 0. \tag{21}$$

Consequently, the asymptotic drag force scales as

$$F \propto \frac{(I_p I_w)^{1+\varphi}}{I_b^{\varphi}} \quad \text{with } \varphi = -\frac{1+\mu+\gamma}{2+\mu+\gamma+\alpha-\beta}. \tag{22}$$

We are interested in the scaling of the drag force with the velocity U_0, which only appears in the flow pressure invariant through $I_p \propto p_0 \propto U_0^2$. Therefore, F scales as $U_0^{2+2\varphi}$ and the asymptotic Vogel exponent naturally appears as $\nu_\infty = 2\varphi$. Ultimately,

$$\nu_\infty = -2\frac{1+\mu+\gamma}{2+\mu+\gamma+\alpha-\beta}. \tag{23}$$

For a uniform, linearly elastic, rectangular plate bending in a uniform flow, $(\alpha,\beta,\gamma,\mu) = (1,0,0,0)$, so that $\nu_\infty = -2/3$, which is

consistent with Alben et al. (2002, 2004) and Gosselin et al. (2010). In the case of a non-linear stress–strain relationship $\sigma \propto \varepsilon^{1/N}$ considered in de Langre et al. (2012), we get $\alpha = 1/N$ in our model, and so we recover the asymptotic result $\nu_\infty = -(2N)/(2N+1)$.

If it is well known that the effects of flexibility are negligible below $C_Y \sim 1$, no study has ever predicted, to the authors' knowledge, the threshold above which the Vogel exponent should finally reach its asymptotic value. This threshold can however be estimated by looking at the global balance of forces on the beam. Assuming that the beam length L loses its relevance when the beam is highly bent implies that there must exist a smaller region of length ℓ, function of the level of loading only, on which all the significant interactions between the beam and the flow concentrate. This inner region is thus responsible for the dominant contribution to the drag, and show a large curvature responsible for the balancing force. Assuming that the contribution of the region $s > \ell$ to the drag is negligible, (15) gives the dominant contribution to the drag as

$$F \sim p_0 w_0 L \ell^{1+\mu+\gamma}. \tag{24}$$

On the other hand, using (3), (2), (11) and (12), the internal shear force at the base can be roughly estimated as

$$f_n(0) \sim b_0 \ell^\beta (L\ell)^{-1-\alpha} = b_0 L^{-1-\alpha} \ell^{-1-\alpha+\beta}. \tag{25}$$

Balancing these two quantities yields

$$\ell^{-(2+\mu+\gamma+\alpha-\beta)} \sim \frac{p_0 w_0 L}{b_0 L^{-1-\alpha}}, \tag{26}$$

which is the Cauchy number defined in Eq. (14). We now choose the specific value of ℓ as follows:

$$\ell = C_Y^{-(1/(2+\mu+\gamma+\alpha-\beta))}. \tag{27}$$

This analysis highlights the emergence of an intrinsic characteristic length ℓ that characterizes the region of the beam on which the interactions governing its behaviour concentrate. Note that this length differs from the effective length used in Luhar (2012). If ℓ is larger than 1 (or equivalently $C_Y < 1$), the flow interacts with the beam on its whole length and the structural behaviour is close to that of a rigid beam. On the other hand, if $\ell \ll 1$, then the interactions in the region of length ℓ dominate the behaviour of the beam, and so the asymptotic regime is reached. This regime, where the Vogel exponent given by (10) has become constant, should thus be expected to be obtained above a threshold that is expressed in terms of some critical value of ℓ instead of C_Y. Depending on the exponent of the power law relating ℓ to C_Y, the gap between the onset of significant bending ($C_Y = 1$) and the convergence of the asymptotic regime ($\ell \ll 1$) might cover a wider or smaller range of loadings. This analysis is consistent with the dimensional analysis above. Indeed, injecting (27) into (24) and using the fact that the pressure of reference p_0 and the Cauchy number C_Y both scale as U_0^2 easily yields

$$F \sim U_0^{2-2((1+\mu+\gamma)/(2+\mu+\gamma+\alpha-\beta))}, \tag{28}$$

and so the asymptotic Vogel exponent given by Eq. (23) is obviously recovered.

Note that the choice of expression (27) to define ℓ is somewhat arbitrary, as no actual "bending length" can be uniquely defined on the physical system. Eq. (27) essentially represents a scaling of the Cauchy number that transforms a ratio of forces into the ratio of some characteristic bending length over the length of the beam. As such, it gives a different interpretation of the Cauchy number, but it does not correspond to a physical quantity that can be easily measured or obtained as the output of a numerical simulation.

4. Applications

4.1. Numerical method

To check the validity of our Eq. (23) for the asymptotic Vogel exponent as well as the predicted threshold discussed above, we numerically compute the Vogel exponent in different cases by solving (13). To solve the integrodifferential equation, we use a first order centred finite difference scheme with the discrete boundary conditions $\theta_1 = 0$, $\theta_{N+1} - \theta_N = 0$ (Thomas, 1995). The integrals are computed by the trapezoidal rule. The resulting non-linear system of equations is solved using a pseudo-Newton solver (so-called method of Broyden, see Broyden, 1965). The beam is discretized with $N = 30$ panels. For $C_Y \leq 1$, the beam bends very little, so we use a uniform mesh. When the beam reconfigures significantly, we have seen that its curvature tends to concentrate in a small region of characteristic non-dimensional length ℓ near the clamped edge. In order to model the curved region with accuracy when $C_Y \geq 1$, we use a non-uniform mesh $s_k = (k/(N+1))^\chi$ with $\chi = \log \ell / \log 2$ so that $s_{((N+1)/2)} = \ell$, meaning that half of the points are in the curved region $s \leq \ell$. This mesh scales with the characteristic bending length in the curved region, and so it is not necessary to increase the number of points to maintain a good accuracy when the beam is highly bent. Convergence was checked on a few cases by measuring the relative error on the asymptotic Vogel exponent. On all the cases tested, doubling the number of points changed the value of the asymptotic Vogel exponent by less than 0.1%.

4.2. A uniform beam in a shear flow

One first situation that is of particular interest is the case of reconfiguration in a sheared flow. This situation is observed for instance for aquatic organisms in underwater boundary layers or within canopies (see Luhar, 2012). We consider a plate of constant width W and cross-section drag coefficient C_D, made of a linearly elastic material of uniform bending stiffness EI, deforming in a flow of uniform density ρ with a sheared velocity profile:

$$U = U_0 \left(\frac{z}{L}\right)^{\mu/2}. \tag{29}$$

Assuming Taylor's model for the local fluid load, the parameters of the model specifically read

$$p(z) = \frac{1}{2}\rho U_0^2 \left(\frac{z}{L}\right)^{\mu}, \quad w(s) = C_D W, \quad c(\theta) = \cos^2\theta, \quad b(s) = EI, \quad g(\kappa) = \kappa, \tag{30}$$

which corresponds to a constitutive law, stiffness and cross-section shape exponents respectively $(\alpha, \beta, \gamma) = (1, 0, 0)$ with the shear exponent μ being the only varying parameter. Hence, from (23), the theoretical asymptotic Vogel exponent is predicted as

$$\nu_\infty = -2\frac{1+\mu}{3+\mu}. \tag{31}$$

In the case of a uniform flow $\mu = 0$, we recover the classical $\nu_\infty = -2/3$ of Gosselin et al. (2010). From (27), the characteristic bending length reads here

$$\ell = C_Y^{-(1/(3+\mu))}. \tag{32}$$

To numerically confirm these predictions, we solve the non-dimensional governing equation Eq. (13) that reads in this specific case:

$$\left.\frac{\partial^2\theta}{\partial s^2}\right|_{s^*} = -C_Y \int_{s^*}^{1} \left(\int_0^s \cos\,\theta(s')\,ds'\right)^{\mu} \cos^2\theta(s)\,\cos\left(\theta(s)-\theta(s^*)\right)\,ds, \tag{33}$$

with the Cauchy number

$$C_Y = \frac{\rho U_0^2 C_D W L^3}{2EI}. \tag{34}$$

Fig. 3 shows the results of the computational approach. In Fig. 3a, the deflection of the beam for increasing loads is shown in the case of a linear flow $\mu/2 = 1$. As expected, significant bending is observed when $C_Y > 1$. The evolution of the reconfiguration number and of the Vogel exponent in Fig. 3b and c stresses the existence of two asymptotic regimes. At low Cauchy numbers, the structure behaves as a rigid beam so the Vogel exponent is null no matter the flow profile. At very large Cauchy numbers however, the Vogel exponent converges towards a constant that depends on the shear exponent μ. The asymptotic Vogel exponent numerically obtained for varying flow profiles is plotted in Fig. 10 in the Appendix, for $C_Y = 10^5$ (which implies $\ell = 0.02$ for $\mu/2 = 0$ and $\ell = 0.2$ for $\mu/2 = 2$). It shows excellent agreement with the theoretical value given by (23). We re-plot in Fig. 4 the evolution of the Vogel exponent as a function of the characteristic bending length ℓ given by (32) instead of the Cauchy number C_Y. In the three cases displayed, the Vogel exponent was within 2% of the asymptotic value for $\ell < 0.2$. This confirms that the threshold for the asymptotic regime is well expressed, for any value of the parameter μ, in terms of the same critical value of ℓ.

The asymptotic results shown in Fig. 10 contradict the preliminary results of Henriquez and Barrero-Gil (2014). The origins of these discrepancies are discussed in the Appendix.

4.3. A uniform beam in a Blasius boundary layer

The particular power-like form of the pressure, cross-section shape and stiffness distributions $p(z)$, $w(s)$, $b(s)$, as well as the constitutive law $g(\kappa)$, is a necessary assumption for the theoretical derivation of the asymptotic expression (23) that may appear like a strong limitation of the model above. It seems however that the actual scope of applicability of (23) encompasses a much wider range of practical situations. For highly bent structures, the curvature tends to concentrate in a small "inner" region $s < \ell$ near the clamped edge. As explained in Alben et al. (2002, 2004), the "outer" portion of the system located above ℓ "sits" in the wake created by the deflection of the incident flow heading to the inner region upstream, and so it only endures very little fluid loading. Consequently, the outer domain only has negligible influence on the overall shape and drag of the structure, and only the spatial dependency of the flow and structural parameters inside the inner domain is actually relevant to the modelling of the system. The whole theory above should thus remain valid as long as power function approximations can accurately model these parameters at the scale of ℓ only, and not necessarily at the scale of the whole beam length.

To better understand the implications above, we consider the reconfiguration of a non-tapered, elastic, homogeneous beam, in a Blasius boundary layer. In this case, all the structural parameters are spatially invariant, but the flow exhibits a more intricate shear profile than a simple power-law fit in z. For the sake of clarity, all the space variables have been

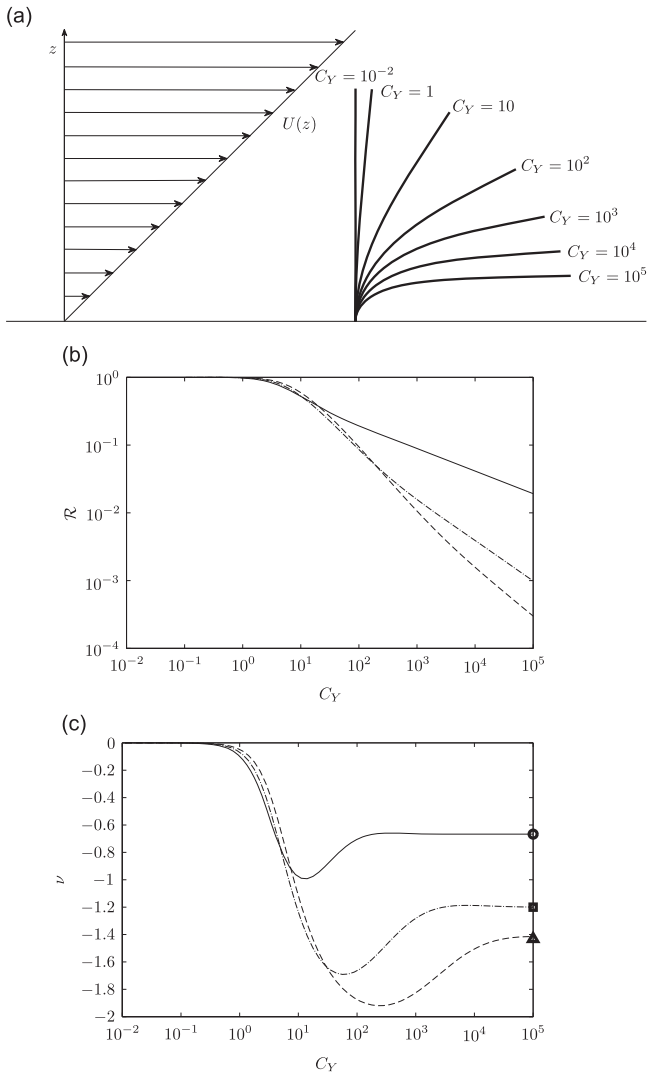

Fig. 3. A uniform beam in a shear flow. (a) Deformation of the beam in a linear flow profile $\mu/2=1$. (b) and (c) Reconfiguration number $\mathcal{R}$ and Vogel exponent ν as functions of the Cauchy number C_Y: uniform flow profile $\mu/2=0$ (——), linear flow profile $\mu/2=1$ (– · –), and quadratic flow profile $\mu/2=2$ (– – –). Asymptotic Vogel exponent predicted by Eq. (23), uniform flow profile $\mu/2=0$ (○), linear flow profile $\mu/2=1$ (□), and quadratic flow profile $\mu/2=2$ (△).

normalized by the length of the beam, or equivalently $L=1$. In the model of Blasius, the vertical velocity is negligible and the horizontal velocity is expressed as

$$U(x,z)=U_\infty f'(\eta), \tag{35}$$

with the similarity variable $\eta=z\sqrt{R_e^L/x}$, the Reynolds number based on the length of the beam and outer flow velocity R_e^L, and f the solution of the Blasius boundary layer equations:

$$2f'''+ff''=0, \quad f(0)=f'(0)=0, \quad f(\eta)\underset{\eta\to\infty}{\longrightarrow}1. \tag{36}$$

The resulting flow profile, shown in Fig. 5a for a fixed value of x, is characterized by a smooth transition from a linear increase with slope $U_\infty/L_B(x)$ near the wall saturating to a uniform magnitude U_∞ far from it. The two domains are roughly delimited, at each location x, by the dimensionless characteristic length scale

$$L_B(x)=\frac{1}{f''(0)}\sqrt{\frac{x}{R_e^L}}, \tag{37}$$

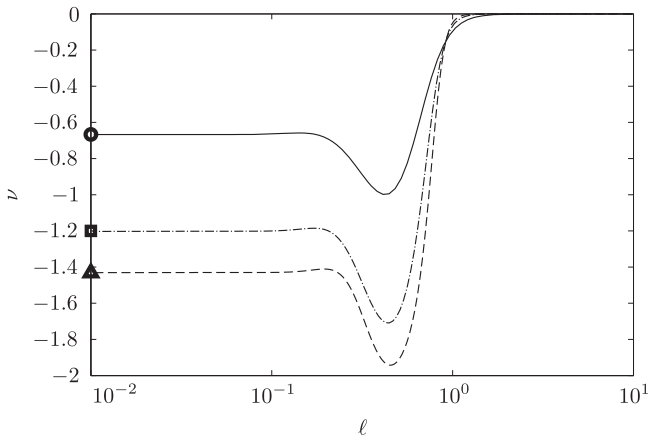

Fig. 4. A uniform beam in a shear flow. Variation of the Vogel exponent in the ℓ–ν space, uniform flow profile $\mu/2=0$ (——), linear flow profile $\mu/2=1$ (– · –), and quadratic flow profile $\mu/2=2$ (– – –). Asymptotic Vogel exponent predicted by Eq. (23), uniform flow profile $\mu/2=0$ (○), linear flow profile $\mu/2=1$ (□), and quadratic flow profile $\mu/2=2$ (△).

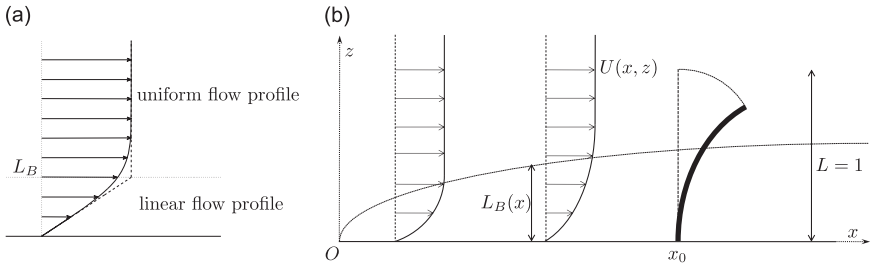

Fig. 5. Description of the reconfiguration in a Blasius boundary layer. (a) Blasius profile $U(x,z)$ at a fixed x. (b) Beam deforming in a Blasius boundary layer.

such that

$$U(x,z)\sim U_\infty \text{ for } z\gg L_B(x) \quad \text{and} \quad U(x,z)\sim \frac{U_\infty}{L_B(x)}z \text{ for } z\ll L_B(x). \tag{38}$$

The approach presented in this paper is based on the assumption that the flow is invariant in the x-direction, and so the x-dependency of the Blasius flow inside the boundary layer would a priori prevent (23) to be valid. However, the region of space swept by the deforming beam extends at most one beam length downstream of its anchorage point x_0 (see Fig. 5b). If the structure is placed far enough from the origin of the boundary layer ($x_0\gg 1$), then $L_B(x)\sim L_B(x_0)$ anywhere in the vicinity of the beam, and so the flow can be considered locally horizontally invariant. The coexistence of the two flow regimes along the vertical axis makes room for two different characteristic velocities according to (38): $U_0=U_\infty$ in the uniform domain, and $U_0=U_\infty/L_B$ in the linear domain. Two Cauchy numbers can subsequently be defined according to (14): $C_{Y,uni}$ is based on the uniform outer flow velocity $U_0=U_\infty$, while $C_{Y,lin}=C_{Y,uni}/L_B^2$ is based on the inner characteristic velocity $U_0=U_\infty/L_B$. Fig. 6a displays the evolution of the Vogel exponent as the loading increases, for several fixed values of $L_B\le 1$. The parameter chosen to describe the fluid loading is the Cauchy number based on the uniform outer flow, $C_{Y,uni}$.

Evidently, if $L_B\ge 1$, then the beam lies entirely in a linearly sheared flow even when it stands upright. This situation is strictly equivalent to the shear flow case studied in Section 4.2 with pressure shear exponent $\mu=2$, if the Cauchy number C_Y is identified with the linear flow Cauchy number $C_{Y,lin}$. For $L_B=1$, $C_{Y,lin}=C_{Y,uni}$ and the evolution of the Vogel exponent shown in Fig. 6a, is very similar to the curve obtained for a linear velocity profile in Fig. 3c.

On the other hand, structures reconfiguring in boundary layers smaller than their length ($L_B<1$) experience much more intricate behaviours. Fig. 6b shows a zoom on the near-wall region of a beam reconfiguring in a Blasius boundary layer a hundred times smaller than its size ($L_B=10^{-2}$). This plot should be analysed jointly with the corresponding curve in 6a. When the Cauchy number is small, the linear flow region is much smaller than the portion of the beam that experiences significant bending. The inner domain $s<\ell$ is mostly subjected to the uniform flow $U=U_\infty$, and the influence of the linear flow on the very bottom of the beam is negligible. Consequently, the evolution of the Vogel exponent for $C_{Y,uni}<10^2$ is very similar to that obtained for a uniform flow in Fig. 3c. As the loading increases, the beam bends more and more and as a result the linear flow covers an increasing portion of the inner region. It follows that the Vogel exponent decreases for $C_{Y,uni}>10^2$. Asymptotically, when the bending region is fully confined inside the boundary layer, the Vogel exponent catches up with the asymptotic value characteristic of linear shear, $\nu_\infty=-6/5$. The same analysis remains valid for other boundary layers smaller than the beam $L_B<1$. If the loading increases enough, the beam will always eventually dive entirely

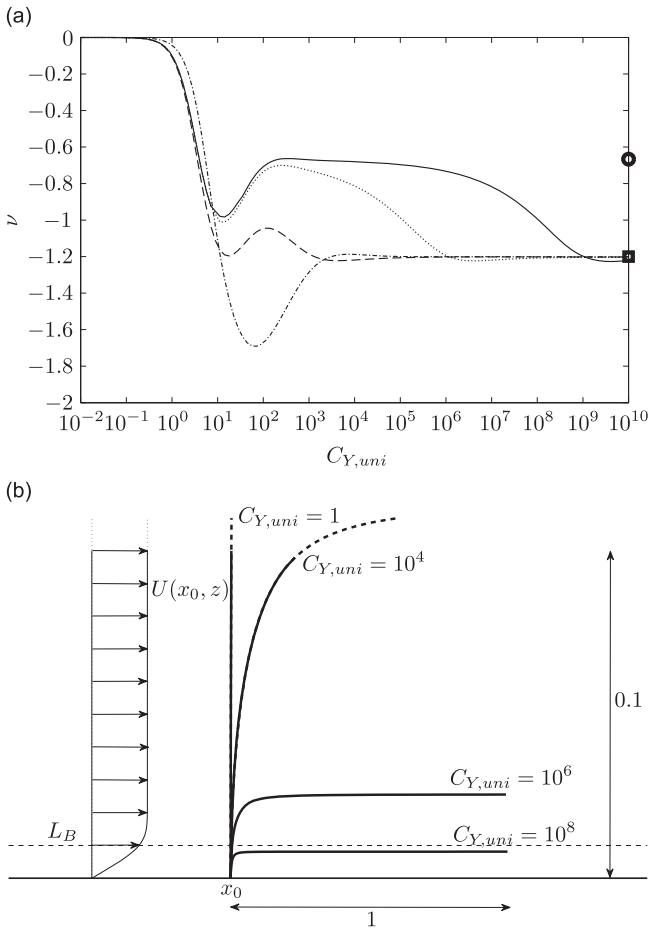

Fig. 6. Reconfiguration in a Blasius boundary layer, anchorage point $x_0 = 10^7$. (a) Vogel exponent ν as a function of the Cauchy number $C_{Y,uni}$, $L_B = 10^{-3}$ (——), $L_B = 10^{-2}$ (· · ·), $L_B = 10^{-1}$ (– – –), and $L_B = 1$ (– · –). Asymptotic Vogel exponent predicted by Eq. (23), uniform flow profile (○), and linear flow profile (□). (b) Zoom near the clamped edge of a beam bending in a Blasius boundary layer, $L_B = 10^{-2}$.

inside the boundary layer and the Vogel exponent will asymptotically reach the theoretical value predicted for a linear flow profile. But the threshold above which this asymptotic regime is reached depends on the thickness of the boundary layer L_B. The larger L_B, the sooner the shear flow will dominate. Precisely, the relative impacts of the uniform and linear flow regions can be estimated by comparing the thickness of the boundary layer L_B to the size of the bending region ℓ. However, the expression of ℓ depends on which of the uniform or linear flow dominates. In the uniform outer flow, (27) yields $\ell_{uni} = C_{Y,uni}^{-1/3}$, while in the linear region it would predict $\ell_{lin} = C_{Y,lin}^{-1/5} = L_B^{2/5} C_{Y,uni}^{-1/5} = L_B^{2/5} \ell_{uni}^{3/5}$. At the threshold between the two regimes, $\ell_{uni} = \ell_{lin} = L_B$, which also yields $C_{Y,uni} = L_B^{-3}$. Note that this threshold specifically sets the lower bound (in terms of the Cauchy number) to the purely linear flow approximation, but the purely uniform flow approximation loses its validity for much smaller loads. Indeed, for ℓ smaller but close to L_B, the region of the beam that concentrates the interaction with the flow is already confined inside the boundary layer so that the influence of the uniform domain above totally vanishes. Conversely, for $\ell > L_B$, the influence of the linear domain never strictly vanishes, and its influence becomes negligible only for $\ell \gg L_B$. This result is consistent with the thresholds for convergence towards the linear regime observed for the different cases in Fig. 6a. For L_B equal to $10^{-1}, 10^{-2}$ and 10^{-3}, the Vogel exponent was within 2.5% of its expected asymptotic value $\nu_\infty = -6/5$ for $C_{Y,uni}$ respectively superior to $10^{2.9}$, $10^{5.85}$ and $10^{8.8}$. If the thickness of the boundary layer L_B is small enough, the influence of the linear region may remain negligible for loadings large enough to permit convergence of the Vogel exponent in the uniform domain, before it reaches the linear domain. This is observed for instance in Fig. 6a, where the Vogel exponent for $L_B = 10^{-3}$ displays a plateau around the asymptotic uniform flow Vogel exponent $\nu = -2/3$ for $C_{Y,uni} \sim 10^2 - 10^5$, before switching to the asymptotic linear flow Vogel exponent $\nu_\infty = -6/5$ above $C_{Y,uni} \sim L_B^{-3} = 10^9$. On the other hand, for thicker boundary layers ($L_B \geq 10^{-2}$), the influence of the linear domain may not be neglected for loadings large enough to reach convergence in the uniform domain. For $L_B = 10^{-1}$, convergence to the asymptotic regime is approximately concomitant with the switch from uniform to linear flow regime. The small hump around $C_{Y,uni} = 10^2$ illustrates the successive dominance of the uniform flow that tends to bring the Vogel exponent closer to $\nu = -2/3$ as the asymptotic regime approaches, soon overcome by the linear flow whose influence is to decrease it to $\nu = -6/5$. When

$L_B = 1$, the linear flow region dominates as soon as reconfiguration occurs, so the early effects of the uniform domain are not even noticeable in Fig. 6a.

This example shows that our approach based on self-similarity actually provides understanding of the behaviour of much more complex configurations. Strictly speaking, there will always be an asymptotic regime, should it be reached for extremely large Cauchy numbers. Indeed, as the structure bends, curvature always concentrate in a region of characteristic length ℓ that gets smaller and smaller, so that it eventually gets small enough for all the parameters to be well approximated by power laws at its scale. Thus, the actual asymptotic Vogel exponent is given by (23) using the exponents of the first order in the power law expansions of the structural and flow parameters at the foot of the beam. Yet, the threshold above which these power law approximations all hold may be too large to be ever reached in practice. In this case, intermediate asymptotic regimes may arise on whole ranges of Cauchy numbers. We may conclude that convergence of the Vogel exponent towards a constant independent of the loading may occur if the bending length ℓ is either much larger or much smaller than any of the other characteristic length scales involved.

4.4. A non-uniform beam in a uniform flow

To further check the validity of the asymptotic expression (23), we compared it to the numerically computed asymptotic Vogel exponent in some other cases involving variations of the material constitutive law, material stiffness or structural cross-section shape. To make sure that the asymptotic regime was reached in the numerical simulations, a large enough value of the Cauchy number ($C_Y = 10^5$) was chosen so that the characteristic bending length ℓ would be inferior to 0.1 in all cases. The results are shown in Table 2, along with the corresponding ℓ-value. Agreement is excellent in all the cases considered.

A more intricate example is that of a linearly tapered beam of increasing width W, namely

$$W(s) = W_1 + (W_0 - W_1)s, \tag{39}$$

as shown in Fig. 7. In most cases, we would then expect the bending stiffness to also vary, but to highlight the effect of the cross-flow area alone, we assume here that the variations of the cross-sectional shape and elastic modulus are chosen such that the bending stiffness remains uniform. Consistently with (14), we define the Cauchy number as in Eq. (34) using the width at the tip W_0 as characteristic width. Note that the case $W_0 - W_1 = 0$ corresponds to the constant width problem $\gamma = 0$, while the case $W_1 = 0$ corresponds to the linear width problem $\gamma = 1$. We define the characteristic length δ as shown in Fig. 7,

Table 2
Comparison of the theoretical and numerically computed Vogel exponents for varying systems.

System	α	β	γ	μ	Theoretical ν_∞ (23)	Numerical ν at $C_Y = 10^5$	ℓ-Value (27) at $C_Y = 10^5$
Benchmark case	1	0	0	0	−2/3	−0.6681	0.02
Elastoplatic behaviour	0.5	0	0	0	−0.8	−0.8013	0.01
Rigid base	1	−1	0	0	−0.5	−0.5006	0.06
Linear width	1	0	1	0	−1	−1.0024	0.06

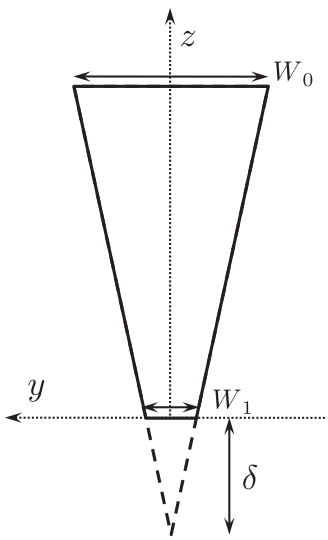

Fig. 7. Tapered beam.

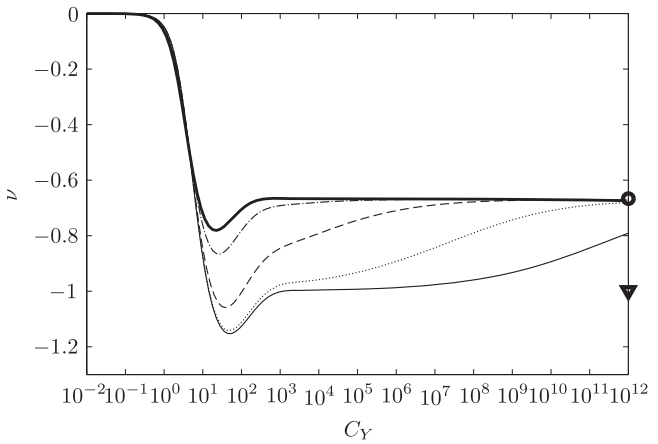

Fig. 8. Vogel exponent ν of a tapered beam for increasing Cauchy numbers C_Y, $\delta = 10^{-3}$ (——), $\delta = 10^{-2}$ (· · ·), $\delta = 10^{-1}$ (− − −), $\delta = 1$ (− · −), and $\delta = +\infty$ (thick ——). Asymptotic Vogel exponent predicted by Eq. (23), constant width (○) and linear width (▽).

such that $W(-\delta) = 0$:

$$\delta = \frac{W_1}{W_0 - W_1}. \tag{40}$$

This quantity can be seen as the length on which the width must vary to significantly deviate from W_1 due to the given slope. Notably, the relative gap between $W(s)$ and W_1 can be expressed as

$$\frac{W(s) - W_1}{W_1} = \frac{s}{\delta}. \tag{41}$$

In other words, the quantity δ is a measure of the length of validity of the uniform width approximation, as L_B was characteristic of the length of validity of the linear flow approximation in the Blasius boundary layer. Hence, the evolution of the computed Vogel exponents shown in Fig. 8 for several values of δ and for increasing Cauchy numbers may be explained in a similar fashion. The Vogel exponent converges at large Cauchy numbers towards the theoretical value $\nu_\infty = -2/3$, consistently with the first order W_1 in the power function expansion (39). For $\delta > 1$, the Vogel exponent deviates very little from that of a beam of uniform width ($\delta = \infty$). Conversely, for very small δ such as 10^{-3}, the structure behaves as a beam of linear width, long enough to exhibit an intermediate asymptotic regime $\nu = -1$ on a broad range of loadings. Structures with intermediate δ-values show an earlier shift from linear-like to uniform-like behaviour that do not allow intermediate convergence of the Vogel exponent. Finally, it should be noted that the characteristic bending lengths reads here $\ell = C_Y^{-1/4}$ in the linear width regime. Hence, the threshold between the two regimes, $\ell/\delta = 1$, reads in this case $C_Y \sim \delta^{-4}$. Contrary to the case of reconfiguration in a boundary layer, this threshold here must be thought of as a reference load around which both the uniform and linear terms of the width (39) influence the behaviour of the beam equally. It is not a critical load above or under which one of the two regimes loses all influence. This is so because, while the two flow domains of the boundary layer were spatially separated (above and below L_B), the two terms of $W(s)$ coexist everywhere, including at the clamped edge. If each term can be neglected, respectively far above or far below the threshold $C_Y = \delta^{-4}$, none of them can be ignored in the transition range around this value. This is consistent with the evolutions displayed in Fig. 8. At $C_Y = \delta^{-4}$, the Vogel exponent is equal to -0.79 for all three values $\delta = 10^{-1}$, 10^{-2} and 10^{-3}.

One may wonder what would happen if the width was decreasing from base to tip instead of increasing. In this case, $\delta < -1$ means that the effects of the slope are only noticeable near the tip, but never near the base where the finite value dominates in any case. In other words, the effects of taper may slightly affect the Vogel exponent for low Cauchy numbers, but the drag rapidly resembles that of a beam of constant width W_1 as soon as bending is significant. These expectations are confirmed by numerical simulations, not shown.

These results shed light on the apparent contradiction between the two asymptotic Vogel exponents for a disk cut along many radii derived respectively by numerical computations ($\nu_\infty = -2/3$) and by dimensional analysis ($\nu_\infty = -1$) in Gosselin et al. (2010). In the latter, it was assumed that because the inner radius R_i was 4–6 times smaller than the exterior radius the small width at the base $W_1 \propto R_i$ could be neglected. However, because the bending stiffness EI, proportional to the width W, cannot vanish at the base, it was assumed that the inner radius still influenced the drag through its finite contribution to the characteristic bending stiffness at the base. Consequently, their analysis corresponds to the case of a purely linear increase of the width from 0 at the base ($\gamma = 1$), on a beam with a non-vanishing bending stiffness ($\beta = 0$), hence the predicted Vogel exponent $\nu_\infty = -1$. However Fig. 8 clearly shows that for δ as small as 10^{-1}, we do not see a plateau at $\nu = -1$ before the effects of the actually non-vanishing width are observed. The two taper ratios considered in Gosselin et al. (2010), $\delta = 0.22$ and 0.32 are even larger, and so the assumption of negligible base width does not hold there. A Vogel exponent of $-2/3$ is in fact to be expected, and that was indeed the result of their numerical computations. Note that the experimental results in

Gosselin et al. (2010) do not match either $\nu = -2/3$ nor $\nu = -1$, neither for the cut-disk nor for the single rectangular plate. The largest Cauchy number considered in the experiments barely exceeded 10^2, so it is very likely that the asymptotic regime was simply not reached. However, the close values of the Vogel exponents computed in both cases ($\nu = -1.3$ for the cut-disk and $\nu = -1.4$ for the rectangular plate) may indicate that the cut-disk behaves similarly to the rectangular plate, consistently with our expectations.

It should also be noted that the influence of other types of tapering was also addressed by Lopez (2012), for slender cones and tree-like structures with rectangular cross-sections (see also Lopez et al., 2014). It was found in both cases that taper had no influence on the scaling of drag, as numerical computations all yielded the same asymptotic Vogel exponent $\nu_\infty = -2/3$. As a matter of fact, as the vertical axis used in these studies was reversed with respect to ours, both the cross-flow width and the thickness of the beam would reach finite values at the clamped edge for any of the geometries considered. Consequently, according to the present study, the drag experienced by such structures in the limit of large loadings scales as that on a beam of uniform properties $(\alpha, \beta, \gamma, \mu) = (1, 0, 0, 0)$. According to Eq. (23), this indeed yields $\nu_\infty = -2/3$.

5. Discussion

5.1. On the use of Eq. (23) for actual systems

Eq. (23) gives the Vogel exponent for large Cauchy numbers in the general case as a function of the exponents α (constitutive law $g(\kappa)$), β (stiffness distribution $b(s)$), γ (cross-section shape distribution $w(s)$), and μ (pressure distribution $p(z)$). Interestingly, (23) can also be written in a simpler form

$$\nu_\infty = -\frac{2}{1+\psi/\phi} \tag{42}$$

that highlights the influence of only two parameters: on the one hand, a *geometrical* parameter $\phi = 1+\mu+\gamma$ that accounts for the distribution of fluid loading on the structure, and on the other hand, a *material* parameter $\psi = 1+\alpha-\beta$ that characterizes the restoring stresses.

In practice, the ranges accessible to the exponents α, β, γ and μ are bounded by limitations of multiple kinds. First, considering the rigid-body force a limiting value, the finiteness of the drag force mathematically requires that $\gamma+\mu > -1$ (see Section 3). But in fact, neither the structural cross-section nor the flow profile of actual systems can possibly diverge at $s=0$, so γ and μ must actually be both positive or null in practice. Moreover, to ensure that the structural stress vanishes for zero curvature, the exponent α of the material constitutive law $g(\kappa)$ has to be strictly positive. Finally, the bending moment at the base cannot vanish when a loading exists. If the stiffness at the base $b(0)$ was null, the curvature there would need to be infinite and the resulting discontinuity in the angle θ across the boundary $s=0$ would make the problem ill-posed. The minimum energy solution would obviously be the straight horizontal beam, which experiences neither drag nor internal stress. To eliminate this case, $b(0)$ must be different from 0, so the exponent β of the self-similar stiffness function $b(s)$ must be negative or null. Note that a system with zero-stiffness at the base would essentially revert to a pin joint free to rotate, with a Neumann boundary condition at $s=0$. This would define a different system that falls out of the scope of this study, and that would experience zero drag no matter the magnitude of the fluid loading. Consequently, the lower physically admissible boundaries for the geometrical and material parameters of our system are $\psi > 1$ and $\phi \geq 1$.

Moreover, practical considerations further set upper boundaries to the typical values expected for these parameters. First, the vast majority of actual structures have finite width, and only quite exotic systems would exhibit cross-sections increasing more than linearly. It also seems unlikely that an actual flow would show more than linear shear, so we may reasonably expect the geometrical parameter ϕ to remain approximately below 3 in most cases. Besides, the constitutive law of most elastic materials should not deviate much from linearity ($\alpha=1$). Even the extreme case of perfect plasticity may be represented by taking $\alpha=0$, as noted by de Langre et al. (2012), and a larger value $\alpha=2$ would already be a very strong exponent. Besides, continuous structures generally show rather smooth variations of their stiffness, so that the magnitude of the exponent of the stiffness distribution, $|\beta|$, should really not deviate much at all from 0. Nonetheless, the use of the present model with $\beta \neq 0$ might constitute a valid approach to handle the overall behaviour of compound or branched structures such as trees. Indeed, the drag of such structure is the sum of the individual drag forces on each of its constitutive elements: trunk, branches, and leaves. The relative contribution of each term is proportional to the projected area of each element. If we model the structure as an equivalent beam with local stiffness based on the weighted mean of the individual elements at a given height, we would expect the equivalent stiffness to decrease by several orders of magnitude from bottom (trunk) to top (leaves). At this point, the validity of this modelling is purely speculative and further investigations should be carried on to analyse its relevance. But in any case, β as low as –1 leads to variations of the stiffness factor that seem already quite sharp for an actual structure, and so we do not expect the material parameter ψ to exceed 3 by much in general.

Considering all these limitations, we may now estimate the expected range of variation of the Vogel exponent. The isovalues of the asymptotic Vogel exponent ν_∞ predicted by (42) are displayed in Fig. 9. They clearly indicate that, in these typical ranges of the geometrical and material parameters $\phi \in [1,3]$ and $\psi \in [1,3]$, ν_∞ may approximately vary between $-1/2$ and $-4/3$ at most. To illustrate the diversity of situations included in this rather narrow parameter space domain, a few practical configurations are marked with crosses on (42). Case A is the benchmark case of Alben et al. (2002, 2004) and Gosselin et al. (2010), where all is

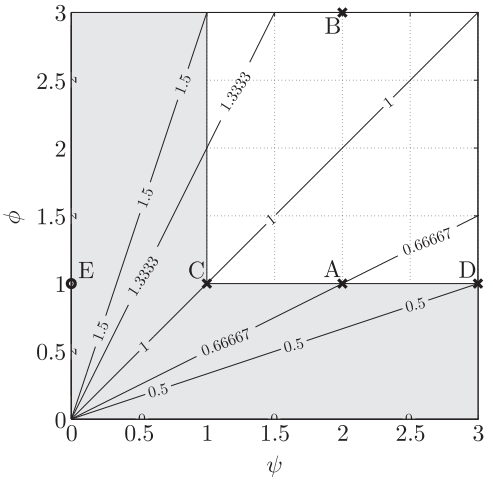

Fig. 9. Absolute value of the Vogel exponent in the reduced parameter space ψ–ϕ. The domain shaded in grey corresponds to non-physical ranges. Practical cases: A–E (see text for the details).

homogeneous and the constitutive law is linear: $(\alpha,\beta,\gamma,\mu)=(1,0,0,0)$. Case B is the linear flow case shown in Fig. 3a: $(\alpha,\beta,\gamma,\mu)=(1,0,0,2)$. Case C would correspond to a uniform, perfectly plastic beam, in a uniform flow: $(\alpha,\beta,\gamma,\mu)=(0,0,0,0)$. Finally, case D would characterize a system with either $(\alpha,\beta,\gamma,\mu)=(2,0,0,0)$ (non-linear constitutive law $g(\kappa)=\kappa^2$) or $(\alpha,\beta,\gamma,\mu)=(1,-1,0,0)$ (global model of a tree with infinite stiffness at the base and flexible branches). Overall, we expect that in most situations of practical interest, the Vogel exponent at large Cauchy numbers will not deviate much from -1. This is consistent with observations on plants, as discussed in the Introduction. Case E will be discussed in Section 5.3.

5.2. On the robustness of the results

The use of Eq. (23) to predict the asymptotic Vogel exponent of a given system relies on the ability to fit a power-law on the spatial distributions of the structural and flow parameters, at least at the scale of the typical length on which significant bending is observed. This requirement may appear as a very limiting factor, because some parameters may exhibit complex variations, and because accurate assessment of the exponents might be challenging. However these two apparent issues might not be as problematic as one might expect.

First, it follows from Sections 4.3 and 4.4 that discrepancies between the actual distributions of the parameters and their best power-law approximations affect very little the validity of the analytical estimation of the Vogel exponent by (23). For instance, it is striking that a beam with taper ratio as large as 10, or even close to 100, still does not exhibit any intermediate plateau similar to the asymptotic regime of a linearly tapered one. In fact, drag reduction on a beam with taper ratio of order 10 is very similar to that of a beam of constant width equal to the base width. Similarly, a structure in a Blasius boundary layer of thickness one order of magnitude smaller than its size is well described, as far as the asymptotic scaling of drag is concerned, by a beam entirely inside the boundary layer. In other words, the ability of (23) to provide accurate estimation of the Vogel exponent of actual systems seems very robust with respect to the accuracy of the self-similar fit of the system parameters. Crude power-law fits at the scale of the bending length are likely to yield rather good results.

Second, the consequences of poor estimations of the exponents of the flow and structural parameter distributions α, β, γ, μ also appear limited. It is noticeable in Fig. 9 that the asymptotic Vogel exponent ν_∞ does not vary much in the domain under consideration. The larger the geometrical and material parameters ϕ and/or ψ, the less sensitive the Vogel exponent becomes to small variations of the parameters. As already noted in de Langre et al. (2012), in the case of a uniform beam in a uniform flow, a quadratic material constitutive law (case D in Fig. 9) is expected to lead to a Vogel exponent of -0.5, which differs very little from the $-2/3$ exponent characteristic of linear elasticity (case A). Similarly, changing a linearly elastic, uniform beam from a linearly sheared flow (case B, $\mu=2$ so $\phi=3$) to an environment with half less shear ($\mu=1$ so $\phi=2$) would only reduce the Vogel exponent from $-6/5$ to -1. Hence, the estimation of the asymptotic Vogel exponent given by (23) is expected to be also robust with respect to the possible errors made in estimating the fitting exponents.

To conclude, it may be said that the prediction of the Vogel exponent using Eq. (23) is quite robust with regard to the parameters of the model.

5.3. On the limits of the model

The whole theory derived in this paper is based on assumptions of three different natures.

First, assumptions have been made regarding the way the action of the flow on the deforming structure is handled. The choice of the simplified form for the local fluid loading (4) has already been discussed in Section 2. As to the specific form of the

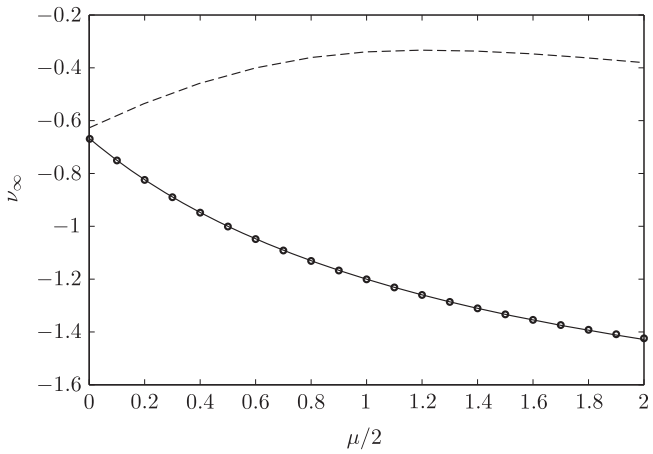

Fig. 10. Asymptotic Vogel exponent ν_∞ for large Cauchy numbers as a function of the flow profile exponent $\mu/2$. Henriquez and Barrero-Gil, 2014 (– – –), present results given by Eq. (23) (——), and numerical simulations at $C_Y = 10^5$ (o).

projection term in the fluid loading distribution $c(\theta) = \cos^2\theta$ used all along the present study following Taylor (1952), alternative admissible forms $c(\theta) = \cos^n\theta$ with $n \geq 1$ were numerically tested, and did not lead to any significant alteration of the results.

Second, the study is limited to the influence of the steady background flow at large Reynolds number, in an otherwise force-free environment. Namely, other effects such as gravity, viscosity, vortex shedding or dynamic effects have been neglected here. Depending on the situation, these additional forces may impact the Vogel exponent of natural systems and explain some of the scattering noted in the measurements performed on actual biological or man-made systems. Yet, consistently with the results of Luhar and Nepf (2011) and Zhu (2008), we do not expect that the present results will be largely affected by the effects of gravity or viscosity. The field of dynamics however still requires further investigations (see Kim and Gharib, 2011 or Luhar, 2012).

Third, as to the type of system chosen, we have considered exclusively the reconfiguration of flexible cantilever beams in cross-flow. Eq. (23) might actually remain valid for a broader range of systems, if the mechanism of reconfiguration is resemblant enough to the axial bending considered here. Formula (42) directly embodies the competition between the fluid loading, characterized by the geometrical parameter ϕ, and the structural restoring force, characterized by the material parameter ψ. All along this paper, we have considered the restoring force to be the internal elastic bending force, but it might very well be of a different nature. For instance, Barois and de Langre (2013) showed that a ribbon with a weight at one end exhibits a constant drag. In that case, the fluid loading is of the same nature as in the present study, but the restoring force is the constant axial tension due to the weight. For such system, the material parameter is $\psi=0$ because there is no length scale associated with the restoring force. It lies out of the admissible range defined earlier, and Eq. (42) yields an asymptotic Vogel exponent $\nu_\infty = -2$ (case E in Fig. 9). This does indeed correspond to a constant drag. Conversely, there does not seem to be any obvious analogy between the present study and the rolling up of sheets cut along one radius treated by Schouveiler and Boudaoud (2006) and Alben (2010). In their case, drag reduction is the result of a more complex three dimensional bending process that does not resemble the mechanism considered here.

Finally, it should be noted that the approach used here may easily be adapted to assess the asymptotic effect of elastic reconfiguration on other physical quantities such as the torque at the base of the structure. After some straightforward calculations, the analytical expression found for the Vogel exponent is similar to (42) except that the geometrical and material parameters ϕ and ψ must be respectively replaced by $1+\phi$ and $1+\psi$.

6. Conclusions

To conclude, we may say that this work provides a framework for the understanding of the typical values of Vogel exponents observed in nature. It was shown that the scaling of drag with respect to the flow velocity, in the limits of large loadings, mostly depends on the best power-law approximation of the flow and structural parameter distributions at the scale of the length on which significant bending occurs. An analytical formula relating the asymptotic Vogel exponent to the fitting exponents was derived in Eq. (23), and the sensitivity of this expression with respect to the accuracy of the modelling was shown to be weak.

More importantly, the application of Eq. (23) to a variety of actual systems highlighted the fact that scattering of the Vogel exponents due to non-uniformities in the structural or flow distributions is expected to remain small. Consistently with experimental observations, the predicted Vogel exponents for large loadings always lie around -1. Consequently, the scaling of the drag on bending beams appears as a characteristic of the mechanism of elastic reconfiguration that depends only on a very limited extent on the actual features of the system. The present study is however limited to quasi-static

configurations. The effects of possible coupling between the structural inertia and the flow dynamics, should it be originated by a time-varying background flow or the consequence of unsteady vorticity shedding in the wake of the structure, still remains to be further investigated.

Acknowledgement

The authors would like to acknowledge financial support from the DGA/DSTL Grant 2014.60.0005 and fruitful discussions with Nigel Peake from the DAMTP, Cambridge, UK.

Appendix A. Comparison with the results of Henriquez and Barrero-Gil (2014)

The problem of reconfiguration in a sheared flow addressed in Section 4.2 is identical to that treated by Henriquez and Barrero-Gil (2014). However, our results strongly differ from theirs, as illustrated in Fig. 10 and discussed below.

There seem to be several possible causes for these discrepancies. First, the choice of the reconfiguration factor $\mathcal{R}$ in Eq. (9) of Henriquez and Barrero-Gil (2014) is non-classical. The numerator does indeed correspond to the total drag on the elastic structure as in the present paper. Yet, the denominator used in Henriquez and Barrero-Gil (2014) does not represent exactly the force on the rigid body. Second, the Vogel exponent is defined as $\nu = 1/2 \times \partial \log \mathcal{R}/\partial \log C_Y$ instead of $\nu = 2 \times \partial \log \mathcal{R}/\partial \log C_Y$ given in Eq. (10) of the present paper to be consistent with $F \propto U^{2+\nu}$. Besides, we believe their numerical solution technique might not be as accurate as ours. As explained in Section 4.1, the inhomogeneous bending along the beam axis makes their choice of uniform mesh with 20 discretization points ill-suited to the large deformation cases investigated here. Finally, the largest Cauchy numbers investigated in Henriquez and Barrero-Gil (2014) do not exceed 10^4, and their definition of the Cauchy number does not include the contribution of the drag coefficient C_D which they choose as 0.4. Hence, the asymptotic results they show correspond to a value of $C_Y \simeq 10^{3.6}$ in our simulations. This does not reach the asymptotic regime for the largest shear exponents.

The very good fit shown in Fig. 10 between our numerical simulations and our Eq. (23) strengthens our confidence in the results of the present study.

References

Alben, S., 2010. Self-similar bending in a flow: the axisymmetric case. Physics of Fluids 22 (8), 081901.
Alben, S., Shelley, M., Zhang, J., 2002. Drag reduction through self-similar bending of a flexible body. Nature 420 (6915), 479–481.
Alben, S., Shelley, M., Zhang, J., 2004. How flexibility induces streamlining in a two-dimensional flow. Physics of Fluids 16 (5), 1694–1713.
Audoly, B., Pomeau Y., 2010. Elasticity and Geometry: From Hair Curls to the Non-Linear Response of Shells. Oxford University Press, Oxford, UK.
Barois, T., de Langre, E., 2013. Flexible body with drag independent of the flow velocity. Journal of Fluid Mechanics 735, R2.
Broyden, C.G., 1965. A class of methods for solving nonlinear simultaneous equations. Mathematics of Computation, 577–593.
Candelier, F., Boyer, F., Leroyer, A., 2011. Three-dimensional extension of Lighthill's large-amplitude elongated-body theory of fish locomotion. Journal of Fluid Mechanics 674, 196–226.
Chakrabarti, S.K., 2002. The Theory and Practice of Hydrodynamics and Vibration, 20. World Scientific, New Jersey.
de Langre, E., 2008. Effects of wind on plants. Annual Review of Fluid Mechanics 40, 141–168.
de Langre, E., Gutierrez, A., Cossé, J., 2012. On the scaling of drag reduction by reconfiguration in plants. Comptes Rendus Mecanique 340 (1), 35–40.
Gosselin, F., de Langre, E., Machado-Almeida, B., 2010. Drag reduction of flexible plates by reconfiguration. Journal of Fluid Mechanics 650, 319–341.
Harder, D.L., Speck, O., Hurd, C.L., Speck, T., 2004. Reconfiguration as a prerequisite for survival in highly unstable flow-dominated habitats. Journal of Plant Growth Regulation 23 (2), 98–107.
Henriquez, S., Barrero-Gil, A., 2014. Reconfiguration of flexible plates in sheared flow. Mechanics Research Communications 62, 1–4.
Kim, D., Gharib, M., 2011. Flexibility effects on vortex formation of translating plates. Journal of Fluid Mechanics 677, 255–271.
Lighthill, M.J., 1971. Large-amplitude elongated-body theory of fish locomotion. Proceedings of the Royal Society of London. Series B. Biological Sciences 179 (1055), 125–138.
Lopez, D., 2012. Modeling Reconfiguration Strategies in Plants Submitted to Flow (Ph.D. thesis). Ecole Polytechnique.
Lopez, D., Michelin, S., de Langre, E., 2011. Flow-induced pruning of branched systems and brittle reconfiguration. Journal of Theoretical Biology 284 (1), 117–124.
Lopez, D., Eloy, C., Michelin, S., de Langre, E., 2014. Drag reduction, from bending to pruning. EPL (Europhysics Letters) 108 (4), 48002.
Luhar, M., 2012. Analytical and Experimental Studies of Plant-Flow Interaction at Multiple Scales (Ph.D. thesis). Massachusetts Institute of Technology.
Luhar, M., Nepf, H.M., 2011. Flow-induced reconfiguration of buoyant and flexible aquatic vegetation. Limnology and Oceanography 56 (6), 2003–2017.
Schouveiler, L., Boudaoud, A., 2006. The rolling up of sheets in a steady flow. Journal of Fluid Mechanics 563, 71–80.
Taylor, G.I., 1952. Analysis of the swimming of long and narrow animals. Proceedings of the Royal Society of London. Series A. Mathematical and Physical Sciences 214(1117), 158–183.
Thomas, J.W., 1995. Numerical Partial Differential Equations: Finite Difference Methods, vol. 22. Springer Science & Business Media, Berlin, Germany.
Tickner, E.G., Sacks, A.H., 1969. Engineering simulation of the viscous behavior of whole blood using suspensions of flexible particles. Circulation Research 25 (4), 389–400.
Vogel, S., 1984. Drag and flexibility in sessile organisms. American Zoologist 24 (1), 37–44.
Yang, X., Liu, M., Peng, S., 2014. Smoothed particle hydrodynamics and element bending group modeling of flexible fibers interacting with viscous fluids. Physical Review E 90 (6), 063011.
Zhu, L., 2008. Scaling laws for drag of a compliant body in an incompressible viscous flow. Journal of Fluid Mechanics 607, 387–400.
Zhu, L., Peskin, C.S., 2007. Drag of a flexible fiber in a 2D moving viscous fluid. Computers & fluids 36 (2), 398–406.